JOURNAL OF MATERIALS SCIENCE **34** (1999) 5721–5732

Sintering mechanisms in strontium doped lanthanum chromite

S. SIMNER*, J. HARDY, J. STEVENSON, T. ARMSTRONG
Materials and Chemical Sciences Department, Pacific Northwest National Laboratory, Richland, WA 99352, USA
E-mail: Steven.Simner@pnl.gov

The sintering behavior of $(La_{0.7}Sr_{0.3})_xCrO_3$ ($0.95 \leq x \leq 1.05$) is investigated to compare liquid phase sintering phenomena occuring in stoichiometric and non-stoichiometric compositions. Shrinkage analysis revealed marked contrast between the densification characteristics of the A-site enriched ($x > 1.00$) and A-site depleted ($x < 1.00$) materials. A-site depleted samples typically exhibited a single liquid phase sintering event at 1250 °C attributed to the melting of an exsoluted $SrCrO_4$ phase. A-site enriched samples indicated two rapid shrinkage events due to the melting of $SrCrO_4$, and a $Sr_{2.67}(CrO_4)_2$ phase with a melting temperature of 1450 °C. $Sr_{2.67}(CrO_4)_2$ was shown to evolve from a decomposition reaction between $SrCrO_4$ and La_2CrO_6, detected together in A-site enriched samples from 800–1000 °C. Maximum densities (93% theoretical density) were achieved for $(La_{0.7}Sr_{0.3})_xCrO_3$ $x = 1.00$ after sintering at 1700 °C for two hours.

1. Introduction

The interconnect in a solid oxide fuel cell (SOFC) is used to electrically connect the anode and cathode of adjacent cells in series. It acts not only as an electrical connection but is also required to separate the reducing atmosphere of the anode from the oxidizing atmosphere of the cathode. As such, the interconnect must be dense (at least 94% theoretical density) to avoid cross leakage of fuel and oxidant gases. In addition to high density, a number of other stringent demands are placed on potential interconnect materials. These include high electronic conductivity ($\rho > 2$ S/cm under reducing conditions at 1000 °C), low ionic conductivity, chemical and mechanical stability (including low volatility and non-reactivity with other cell components) in both oxidizing and reducing atmospheres, matching thermal expansion with the electrodes and electrolyte and the absence of phase changes or impurity phase formation with long operating times at temperatures between 25–1000 °C.

These requirements exclude all but a few oxide systems from consideration. Lanthanum chromite materials satisfy many of the above criteria and have been used as SOFC interconnect materials for over 30 years. However, it is well established that $LaCrO_3$ is difficult to sinter to high density in air. Poor sinterability under oxidizing conditions results from CrO_3 volatilization above 1000 °C [1]. The gaseous CrO_3 condenses at interparticle necks as Cr_2O_3 during the initial stages of sintering. Because neck growth is accomplished without transport of the material from the bulk of the grains, little densification or pore removal occurs. In order to achieve high density the oxygen partial pressure should be controlled at 10^{-12}–10^{-9} atm [2], which is close to the oxygen partial pressures specified by the chromium/Cr_2O_3 phase boundary to suppress grain growth and allow densification to occur [3]. Due to the volatility of CrO_3, $LaCrO_3$ has traditionally been sintered under reducing atmospheres at temperatures greater than 1600 °C to produce high density materials [4].

Several techniques have been investigated to achieve high density $LaCrO_3$ in air. These include the addition of sintering aids, such as fluorides [5], the use of highly reactive powders [6], firing $LaCrO_3$ between Cr_2O_3 plates [7], the addition of alkaline earth elements (e.g. Ca, Sr or Mg [8, 9]), the addition of transition metals (e.g. Zn or Cu [10]), and the use of low melting point eutectic compositions, such as MnO-TiO_2 and Nb_2O_5-V_2O_5, to act as foreign liquid phases [11].

The most promising recent developments have exploited transient liquid phase sintering in slightly non-stoichiometric Ca-doped $LaCrO_3$, commonly termed LCC. An extensive literature review and study of densification mechanisms in LCC compositions have recently been reported by Chick *et al.* [12]. Chick *et al.* [12] investigated the presence of non-perovskite phases in $La_{0.7}Ca_xCrO_3$ with $0.25 \leq x \leq 0.35$, and how such phases might be involved in the sintering of LCC. Samples were heated to temperatures between 800–1530 °C and air quenched for XRD analysis. $CaCrO_4$, exsoluted from the perovskite due to poor alkaline earth solubility below 1200 °C, was detected in abundance at 800 °C in samples with $x > 0.25$.

* Author to whom all correspondence should be addressed.

With increased temperature the $CaCrO_4$ progressively decreases due to redissolution in the perovskite, but sufficient remains to act as a transient liquid phase in all samples on melting. The melting temperature of this phase and subsequent shrinkage was found to be dependent on the stoichiometry of the sample. The shrinkage event began as low as 850 °C for the material with $x = 0.35$, and as high as 1000 °C for the material with $x = 0.29$. In general, the higher temperature shrinkage event occurred in A-site depleted samples, and the lower temperature event in the A-site enriched samples. This dependence of the onset of liquid phase sintering was believed to be associated with the presence of small amounts of La_2CrO_6 observed in A-site enriched samples quenched from 800–1000 °C. DTA was performed on a 80 wt % $CaCrO_4$-20 wt % La_2CrO_6 composition, and indicated a drop in the melting temperature of $CaCrO_4$. It was speculated that La dissolution in the $CaCrO_4$ increased the entropy of the liquid, thereby lowering its melting point. Samples with $x > 0.3$ (A-site enriched) exhibited a second rapid shrinkage event resulting in high density samples. This shrinkage event was not observed in the A-site depleted compositions ($x < 0.3$). The onset of the second liquid formation occurred around 1200 °C and was attributed to the melting of $Ca_3(CrO_4)_2$ (m.p. 1253 °C). Chick *et al.* [12] showed how the sintering behavior was determined by the decomposition, phase changes and redisolution of the minor non-perovskite phases. After melting of $CaCrO_4$ the minor phase composition in the A-site depleted (Cr-enriched) samples moved into a (liquid + β-$CaCr_2O_4$) phase field which became increasingly enriched in solid, thus preventing further liquid phase sintering. However, the minor phase composition of the A-site enriched samples, prior to melting of $CaCrO_4$, was thought to consist of $CaCrO_4$ and $Ca_3(CrO_4)_2$. Melting of these phases at their respective melting points was believed to account for the rapid shrinkage events observed in the A-site enriched LCC samples.

Sr-doped $LaCrO_3$ (LSC) is expected to exhibit similar sintering behavior to LCC materials though little work has been conducted to verify this fact. This is predominantly due to current interest in co-firing the cathode and interconnect; the lower sintering temperature of LCC make it a more attractive candidate. Recent studies, however, have indicated that LCC may not be the most suitable interconnect material due to dimensional instability under reducing atmospheres. Armstrong *et al.* [13] showed that the linear expansion of sintered chromites increased with increasing temperature, with decreasing oxygen partial pressure, with increasing acceptor dopant concentration and with increasing oxygen non-stoichiometry. LCC materials showed greater expansion at low oxygen partial pressures than LSC materials. As such LSC materials have found renewed interest. It is, however, widely recognized that Sr-doped materials do not sinter to high density in air. Chick *et al.* [14] have shown that the sintering of $La_{1-x}Sr_xCrO_3$ is enhanced by Cr-depletion though densities >94% theoretical density were difficult to achieve even above 1500 °C. Therefore, many previous studies have been directed at sintering LSC under low oxygen partial pressures. Meadowcroft [15] reported that densification of $La_{0.84}Sr_{0.16}CrO_3$ was enhanced significantly with the addition of 3 to 5 mol % excess $SrCO_3$ when fired under a reducing atmosphere. Groupp and Anderson [4] were able to produce nearly theoretically dense samples of $La_{1-x}Sr_xCrO_3$ by sintering at 1720 °C with an oxygen activity of 10^{-12}–10^{-11} atm. Mori *et al.* [16] studied sintering mechanisms for $La_{1-x}Sr_xCrO_3$ under reducing atmosphere, and showed that rapid shrinkage around 1900 °C was due to the melting of α-$Sr(CrO_2)_2$. The behavior at low oxygen partial pressures is predicted to be markedly different than that for air sintered materials. Sintering studies for LSC materials in air are limited. Sammes *et al.* [17] have shown that the densification of $La_{1-x}Sr_xCrO_3$ increased with increased Sr content, and that 96% theoretical could be obtained for $La_{0.7}Sr_{0.3}CrO_3$ when fired at 1700 °C in air. Tai and Lessing [7] reported a theoretical density of above 93% for $La_{1-x}Sr_xCrO_3$ when sintered in air sandwiched between two Cr_2O_3 plates and fired at 1700 °C for 7 h.

The most detailed investigation has been conducted by Chick *et al.* [18]. Their studies considered the sintering mechanisms of $La_{1-x}Sr_xCrO_3$ compositions with $0 \leq x \leq 0.24$. For samples $x = 0.0$ and 0.12 shrinkage dilatometry revealed gradual shrinkage with no rapid densification events. At higher Sr dopant levels the shrinkage exhibited three pronounced inflections around 1000, 1250 and 1450 °C. X-ray phase analysis indicated that $SrCrO_4$ (m.p. 1253 °C) was probably responsible for the second rapid shrinkage. Phenomena associated with the inflections in the shrinkage curve at 1000 °C and 1450 °C were undetermined. This study also investigated the effects of non-stoichiometry in $La_{(0.76-y)}Sr_{0.24}Cr_{(1+y)}O_{3-\delta}$ samples. Cr-deficient samples generally exhibited higher sintered densities. The highest density (~95% theoretical density) was achieved for Cr-deficient compositions with an (La + Sr)/Cr ratio of 1.02. An (La + Sr)/Cr ratio of 0.92 yielded only 75% theoretical density. Mechanisms causing the differences in sintering behavior were not discussed.

This present work considers the effects of non-stoichiometry on the sintering behavior of $(La_{0.7}Sr_{0.3})_xCrO_3$ with $0.95 \leq x \leq 1.05$. In order to characterize this behavior a number of analysis techniques have been employed including sintered density measurements, sintering shrinkage dilatometry, powder X-ray diffraction and thermal analysis (DTA-TGA). The first two techniques enable determination of temperatures at which significant sintering of these materials occurs, while the latter analysis methods provide insight into the phenomena responsible for these events.

2. Experimental

Chromite powders were synthesized by the glycine-nitrate process, using a stoichiometric fuel/oxidant ratio [19]. Glycine-nitrate precursor solutions were prepared by combining weighed aliquots of stock solutions

of the individual metal nitrates. The concentrations of the nitrate stock solutions were initially characterized by gravimetric analysis-heating a known weight of nitrate solution to 900 °C to form the respective oxide, and then weighing the oxide formed. This enables concentration of the stock solution to be calculated in terms of the number of moles of metal ion per gram of solution. Gravimetric results were verified by EDTA titration [20]. Gravimetric and EDTA techniques resulted in cumulative errors for the three component precursor solution amounting to approximately 0.5%. The synthesis of each composition was tightly controlled by making large batches (typically > 1 kg) of the combined nitrate solutions, and measuring out each constituent solution to an accuracy of 0.01 g. Compositions investigated in this study were of the general formula $(La_{0.7}Sr_{0.3})_xCrO_3$ where $x = 0.95$, 0.97, 0.99, 1.00, 1.01, 1.03, and 1.05. These compositions will subsequently be referred to as LSC-30, denoting 30 mol % Sr substitution for La on the A-site. The degree of non-stoichiometry is indicated by $x = 0.95$–1.05; e.g. $(La_{0.7}Sr_{0.3})_{0.95}CrO_3$ is denoted by LSC-30 ($x = 0.95$) and $(La_{0.7}Sr_{0.3})_{1.05}CrO_3$ by LSC-30 ($x = 1.05$), etc.

Powder used for sintering shrinkage measurements was calcined at 650 °C for 30 min to remove residual carbon, and pressed into bars ($20 \times 10 \times 5$ mm) uniaxially at 33 MPa and then isostatically at 130 MPa. Sintering shrinkage tests were carried out in a Unitherm Model 1161 vertical pushrod dilatometer with a 40 g load from room temperature to 1600 °C at a heating rate of 2 °C/min.

As a first step in investigating the sintered density-temperature relationship of LSC materials, stoichiometric LSC-30 ($x = 1.00$) was analyzed to determine the optimum calcination temperature for maximum densification during sintering. Powder samples were calcined at temperatures from 650–1200 °C for 1 h. The optimum calcination temperature was established at 800 °C, yielding post-sintered densities of ~93% theoretical. Calcined powders were uniaxially pressed at 33 MPa and isostatically pressed at 130 MPa. Density-temperature relationships were investigated from 1100° to 1700 °C at 100 °C intervals. At each temperature, four samples of each composition were sintered for 2 h, and their densities measured by the Archimedes' method using ethyl alcohol. Relative densities were calculated as a percentage of the theoretical density for each LSC-30 composition, which had been established through X-ray diffraction (XRD) and subsequent unit cell refinement.

XRD analysis was performed on pressed samples which had been air-quenched after heating to temperatures from 800–1600 °C at 100 °C intervals. Quenched samples were crushed, ground and screened through a 200 mesh sieve prior to analysis. X-ray data was recorded between 15° and 80° 2Θ with 0.04° steps, and a 2 s count using a Philips Wide-Range Vertical Goniometer and a Philips XRG3100 X-ray Generator. Additional XRD was conducted on powders, which had been calcined for 1 h at temperatures between 800–1600 °C and allowed to cool slowly in a closed furnace. Semi-quantitative XRD phase analysis was conducted to compare phase development in both quenched and calcined LSC-30 samples. After XRD phase analysis on the LSC-30 compositions was completed, some of the non-perovskite phases detected were synthesized and reacted in various combinations. Unless otherwise stated these phases were produced by the glycine-nitrate process. The resulting products were analyzed using the XRD and DTA/TGA to study the development and interaction of secondary phases in the LSC system.

Differential thermal analysis (DTA) and thermogravimetric analysis (TGA) of the LSC-30 compositions was conducted on a Netzsch Model 409 DTA. Powders were pressed into small discs approximately 5 mm in diameter, typically weighing 50–100 mg. Samples were analyzed from room temperature to 1500 °C with a heating rate of 5 °C/min.

3. Results and discussion

3.1. Sintering characteristics of $(La_{0.7}Sr_{0.3})_xCrO_3$ $x = 0.95$–1.05 compositions

3.1.1. Shrinkage dilatometry

Fig. 1 shows sintering shrinkage curves for LSC-30 compositions. The shrinkage behavior for LSC-30 compositions $x = 0.95$ and 0.97 is almost identical and hence the curve for $x = 0.97$ has been omitted to improve the clarity of the diagram. Rapid shrinkage for compositions $x = 0.95$ and 0.97 occurs around 1250 °C and is consistent with the first two stages of liquid phase sintering, particle rearrangement and solid solution-reprecipitation processes [21]. Subsequent sintering of these samples is more gradual, indicative of solid state diffusion. For LSC-30 $x = 0.99$ and 1.00 the sintering behavior is initially comparable to the $x = 0.95$ and 0.97 samples with significant densification occurring around 1250 °C. However, a second rapid sintering event is observed close to 1580 °C for $x = 0.99$ and 1540 °C for $x = 1.00$. The magnitude of the first shrinkage event is approximately equal for all samples of $x \leq 1.00$ possibly indicating the formation of similar volumes of liquid at 1250 °C.

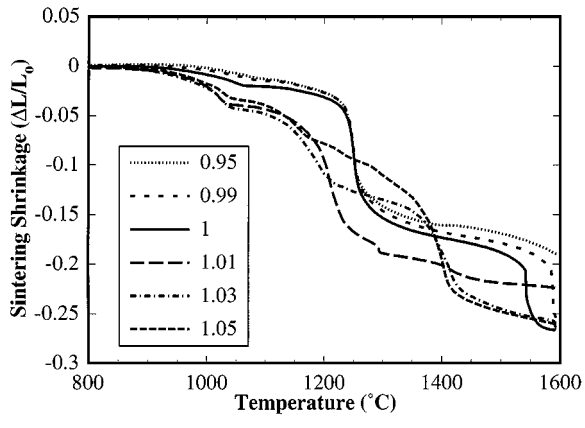

Figure 1 Sintering shrinkage curves of $(La_{0.7}Sr_{0.3})_xCrO_3$ where $0.95 \leq x \leq 1.05$. Data for $x = 0.97$ has been omitted because it exhibits identical shrinkage behavior to $x = 0.95$. Samples were heated at 2 °C/min.

For LSC-30 compositions with $x > 1.00$ the sintering shrinkage behavior varies considerably with respect to compositions of $x \leq 1.00$. The first notable difference is a brief but fairly rapid shrinkage event around 980 °C. More rapid densification occurs at ~1150 °C and the magnitude of this event decreases as A-site enrichment increases. The variation in shrinkage magnitude for these compositions is most likely related to the amount of liquid phase available for sintering. For $x = 1.01$ this is the only major densification phenomena observed, although two additional small kinks in the dilatometer curve are apparent around 1300 and 1400 °C. For $x = 1.03$ the magnitude of the first rapid shrinkage is less than that observed for $x = 1.01$ but a second major event occurs just below 1400 °C. For $x = 1.05$, the shrinkage event beginning around 1050 °C is very brief. Subsequent sintering between 1200–1380 °C takes place gradually, possibly suggesting the formation of small amounts of a number of different liquid phases, but is followed by a sharp increase in the sintering rate around 1400 °C. Although the magnitudes of the major shrinkage events for the A-site enriched samples are different, the temperatures at which they occur (i.e. 960, 1150 and 1400 °C) are identical for each composition. Above 1450 °C, solid state sintering processes appear to dominate for all A-site enriched LSC-30 compositions.

3.1.2. Sintered density

Fig. 2 illustrates the relationship between relative density (i.e. percent of theoretical density) and firing temperature for LSC-30 samples sintered for 2 h from 1100 °C to 1700 °C at 100 °C increments. Error bars are not indicated on the figure because they were smaller than the symbols used to denote the relative density values for each composition. Sintered densities range from 85–93% theoretical at 1700 °C, with the highest densities observed for $x = 0.99$ and 1.00 compositions. The density-temperature relationships for compositions of $x \leq 0.99$ (A-site depleted) are very similar indicating significant densification between 1200–1300 °C and a smaller event between 1500–1600 °C, most pronounced for $x = 0.99$. Sintered density values for $x = 0.95$ and 0.97 were identical and the $x = 0.97$ trace has been omitted. LSC-30 $x = 1.00$ behaves similarly to samples with $x < 1.00$ until 1400 °C. Between 1400–1500 °C enhanced densification occurs for the $x = 1.00$ composition. This does not correlate with the shrinkage data for this sample, which indicates a second rapid shrinkage event around 1540 °C. It is possible that the mechanism responsible for this event is kinetically retarded, and was thus observed at a higher temperature in the shrinkage dilatometry than for sintered density measurements where samples were held at the sintering temperature for 2 h. This will be discussed in greater detail in a later section.

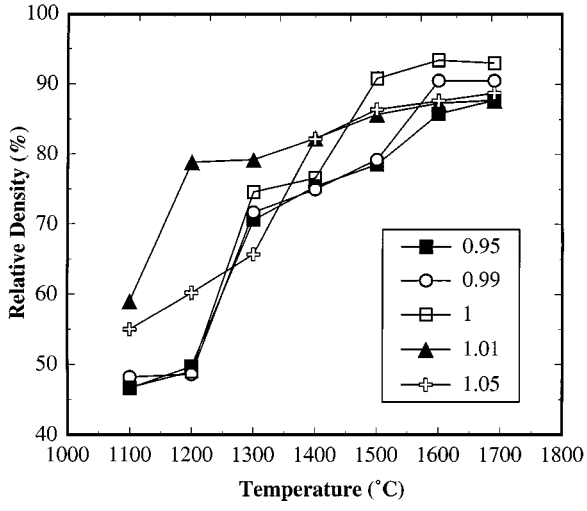

Figure 2 Sintered density data for $(La_{0.7}Sr_{0.3})_x CrO_3$ ($0.95 \leq x \leq 1.05$) after sintering for 2 h at 100 °C intervals between 1100–1700 °C. Data for $x = 0.97$ and 1.03 have been omitted as they follow the curves for 0.95 and 1.05, respectively.

The sintering characteristics of samples where $x > 1.00$ correspond well to shrinkage data. LSC-30 $x = 1.03$ has been excluded from Fig. 2 because its sintering behavior closely resembles that of $x = 1.05$. It is interesting to note that at 1100 °C the densities of $x > 1.00$ compositions are approximately 10% greater than $x \leq 1.00$. This parallels the shrinkage data in Fig. 1, and possibly corresponds to the initial shrinkage event observed around 960 °C for $x > 1.00$ compositions. For $x = 1.01$ the sample reached almost 80% of its theoretical density by 1200 °C, significantly higher than that attained by other compositions at this temperature. This is also verified by shrinkage data indicating $x = 1.01$ to have undergone the highest degree of shrinkage by 1200 °C. For $x = 1.03$ substantial densification occurs between 1100–1200 °C and a more significant event from 1300–1400 °C, as observed in shrinkage analysis. The behavior of $x = 1.05$ is almost identical to $x = 1.03$ with a large proportion of densification occurring between 1300–1400 °C.

Most interesting is the fact that compositions $x = 0.95$ and 0.97 attain equivalent densities to those achieved by the A-site enriched compositions. This is contrary to the shrinkage results presented in Fig. 1, which indicated poor shrinkage for the LSC-30 A-site depleted compositions. However, shrinkage dilatometry was restricted to a maximum temperature of 1600 °C and additional, undetected phenomena may be occurring in the sintered samples above this temperature. Alternatively, the high densities may simply be attributed to solid state sintering during the 2 h hold time at the higher sintering temperatures (1600 and 1700 °C) used.

3.1.3. Phase determination by X-Ray diffraction

Table I indicates the wt % of non-perovskite phases detected by XRD for each LSC-30 composition air quenched from 800–1600 °C. Some phases in Table I, at the higher temperatures investigated, are proceeded by "*T*" rather than a value indicating weight percent. This denotes a trace amount of a phase was detected, though it was difficult to establish the exact proportion of the phase present.

TABLE I Percent by weight of non-perovskite phases present in $(La_{0.7}Sr_{0.3})CrO_3$ ($0.95 \leq x \leq 1.05$) samples quenched in air from 800–1600 °C (T denotes a trace amount)

	$x = 0.95$	$x = 0.97$	$x = 0.99$	$x = 1.00$	$x = 1.01$	$x = 1.03$	$x = 1.05$
800 °C	8.8 $SrCrO_4$	8.7 $SrCrO_4$	8.7 $SrCrO_4$ 1.1 La_2CrO_6	8.5 $SrCrO_4$ 1.3 La_2CrO_6	8.7 $SrCrO_4$ 2.0 La_2CrO_6	10.1 $SrCrO_4$ 2.9 La_2CrO_6	9.3 $SrCrO_4$ 4.6 La_2CrO_6
900 °C	8.6 $SrCrO_4$	8.8 $SrCrO_4$	7.9 $SrCrO_4$	7.7 $SrCrO_4$	8.2 $SrCrO_4$	8.7 $SrCrO_4$ 1.2 La_2CrO_6	9.6 $SrCrO_4$ 1.6 La_2CrO_6
1000 °C	7.4 $SrCrO_4$ 0.5 Cr_2O_3	7.6 $SrCrO_4$ 0.5 Cr_2O_3	7.7 $SrCrO_4$	7.0 $SrCrO_4$	8.0 $SrCrO_4$	7.9 $SrCrO_4$ 2.0 $Sr_{2.67}(CrO_4)_2$	5.3 $SrCrO_4$ 2.2 $Sr_{2.67}(CrO_4)_2$
1100 °C	6.1 $SrCrO_4$ 0.7 Cr_2O_3	4.6 $SrCrO_4$ 0.4 Cr_2O_3	5.4 $SrCrO_4$	4.5 $SrCrO_4$ 1.0 $Sr_{2.67}(CrO_4)_2$	3.8 $SrCrO_4$ 1.1 $Sr_{2.67}(CrO_4)_2$	3.8 $SrCrO_4$ 1.9 $Sr_{2.67}(CrO_4)_2$ 0.8 La_2O_3	2.3 $SrCrO_4$ 3.3 $Sr_{2.67}(CrO_4)_2$ 0.8 La_2O_3
1200 °C	4.2 $SrCrO_4$ 0.9 Cr_2O_3	4.7 $SrCrO_4$ 0.6 Cr_2O_3	4.0 $SrCrO_4$	4.0 $SrCrO_4$ 1.6 $Sr_{2.67}(CrO_4)_2$	2.7 $SrCrO_4$ 1.1 $Sr_{2.67}(CrO_4)_2$	1.9 $SrCrO_4$ 2.4 $Sr_{2.67}(CrO_4)_2$ 0.9 La_2O_3	1.6 $SrCrO_4$ 4.1 $Sr_{2.67}(CrO_4)_2$ 1.3 La_2O_3
1300 °C	3.7 $SrCrO_4$ 0.9 Cr_2O_3	3.4 $SrCrO_4$ 0.8 Cr_2O_3	3.2 $SrCrO_4$ 0.7 $Sr_{2.67}(CrO_4)_2$	2.8 $SrCrO_4$ 1.5 $Sr_{2.67}(CrO_4)_2$	1.1 $SrCrO_4$ 1.3 $Sr_{2.67}(CrO_4)_2$	0.9 $SrCrO_4$ 4.0 $Sr_{2.67}(CrO_4)_2$ 0.9 La_2O_3	0.8 $SrCrO_4$ 4.0 $Sr_{2.67}(CrO_4)_2$ 1.2 La_2O_3
1400 °C	1.6 $SrCrO_4$ 1.0 Cr_2O_3	2.1 $SrCrO_4$ 0.7 Cr_2O_3	1.9 $SrCrO_4$ 1.2 $Sr_{2.67}(CrO_4)_2$ 0.5 Cr_2O_3	1.2 $SrCrO_4$ 1.5 $Sr_{2.67}(CrO_4)_2$	T $SrCrO_4$ 1.3 $Sr_{2.67}(CrO_4)_2$	T $SrCrO_4$ 2.3 $Sr_{2.67}(CrO_4)_2$ 0.8 La_2O_3	T $SrCrO_4$ 2.8 $Sr_{2.67}(CrO_4)_2$ 1.0 La_2O_3
1500 °C	1.0 Cr_2O_3	1.5 $SrCrO_4$ T Cr_2O_3	1.1 $SrCrO_4$ 1.3 $Sr_{2.67}(CrO_4)_2$ T Cr_2O_3	0.8 $SrCrO_4$ 1.2 $Sr_{2.67}(CrO_4)_2$	2.7 $Sr_{2.67}(CrO_4)_2$	4.4 $Sr_{2.67}(CrO_4)_2$	3.2 $Sr_{2.67}(CrO_4)_2$ 1.0 La_2O_3
1600 °C	0.7 Cr_2O_3	T Cr_2O_3	1.3 $Sr_{2.67}(CrO_4)_2$ T Cr_2O_3	0.8 $Sr_{2.67}(CrO_4)_2$	1.9 $Sr_{2.67}(CrO_4)_2$	3.5 $Sr_{2.67}(CrO_4)_2$	2.7 $Sr_{2.67}(CrO_4)_2$ 0.6 La_2O_3

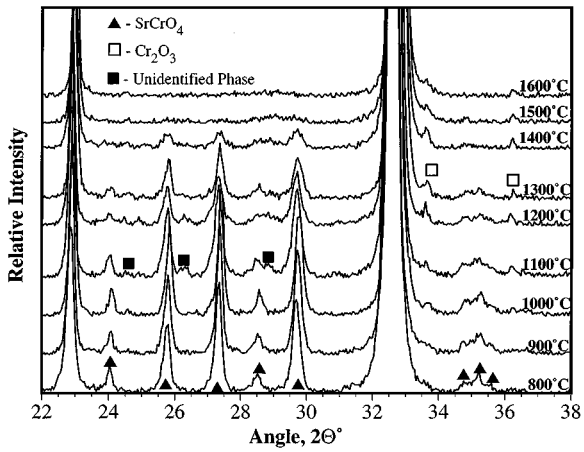

Figure 3 X-ray diffraction patterns of quenched $(La_{0.7}Sr_{0.3})_{0.95}CrO_3$ from 22–38 ° 2Θ indicating non-perovskite phases present between 800–1600 °C.

3.1.3.1. $(La_{0.7}Sr_{0.3})_xCrO_3$ ($x = 0.95$ and 0.97). Shrinkage and sintered density results suggest that these A-site depleted phases are subject to similar sintering phenomena since they both exhibit a single rapid densification event, similar in magnitude, around 1250 °C. XRD analysis substantiates this indicating that the same two non-perovskite phases, $SrCrO_4$ and Cr_2O_3 are present in both $x = 0.95$ and 0.97 compositions. Fig. 3 presents XRD data for LSC-30 $x = 0.95$ samples quenched from 800 °C to 1600 °C. The figure focuses on a 2Θ range of 22–38° indicating high intensity peak positions of the non-perovskite phases. $SrCrO_4$ is the principal non-perovskite phase observed in LSC-30, $x = 0.95$ and 0.97, exsoluted due to poor solid solubility in the perovskite at lower temperatures, and its concentration decreases steadily with increasing temperature as shown in Fig. 3 and Table I. The other non-perovskite phase detected by XRD is Cr_2O_3 (m.p. ∼2275 °C), which first appears around 1000 °C and is still present in trace amounts even at 1600 °C. Fig. 3 also shows a number of unidentified peaks detected by X-rays from 1100 °C to 1300 °C. Similar peaks were observed in the same temperature range for all LSC-30 compositions. These phases are only observed in trace amounts and not detected above 1300 °C. Some of the peaks were tentatively identified as La_4SrO_7. This melts at 2100 °C, and as such is not expected to play a significant role in the sintering of these samples.

The SrO-Cr_2O_3 phase diagram [22] indicates the melting point of $SrCrO_4$ to be 1253 °C, and hence it is reasonable to conclude that this phase is responsible for the first shrinkage event observed for samples $x = 0.95$ and 0.97. Rapid shrinkage for A-site depleted Ca-doped $LaCrO_3$ around 1000 °C, observed by Chick [12] and Carter [23], was similarly attributed to the melting of $CaCrO_4$ (melting point 1022 °C). The melting temperature of $SrCrO_4$ was verified at 1256 °C by DTA analysis of commercially supplied $SrCrO_4$ (Alfa Aesar, 95% purity). Thermal analysis, DTA and TGA, was also performed on a pressed sample (weighing ∼100 mg) of LSC-30 $x = 0.95$ to confirm a melting event around 1250 °C. The recorded data is presented in Fig. 4. An endotherm for the melting of $SrCrO_4$ was observed at 1256 °C, and the small but rapid weight loss at this temperature is assumed to be related to incongruent melting in air of $SrCrO_4$ to liquid and Cr_2O_3, as depicted in the SrO-Cr_2O_3 phase diagram [22]. Oxygen is believed to be lost due to the reduction of Cr^{6+} in $SrCrO_4$ to Cr^{3+} in Cr_2O_3.

There is also a more gradual weight loss evident from 800 °C to 1500 °C. Various LSC compositions were subjected to TGA analysis with 2 heating and 2 cooling events to establish if this weight loss was repeated on reheating. The first heating indicated weight

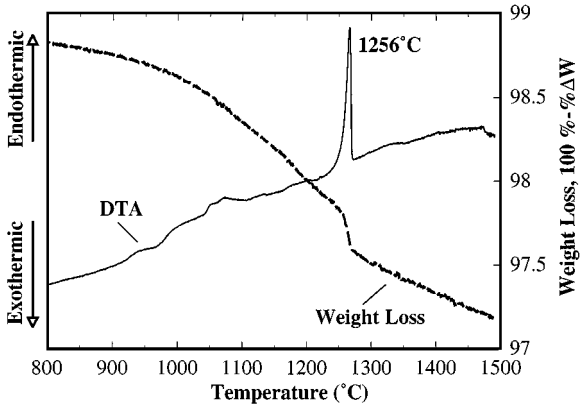

Figure 4 DTA and TGA curves for $(La_{0.7}Sr_{0.3})_{0.95}CrO_3$ indicating the melting of $SrCrO_4$ at 1256 °C.

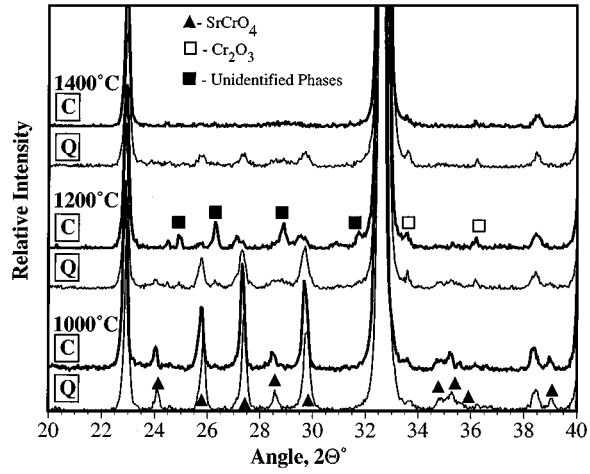

Figure 5 Comparison of X-ray diffraction patterns of quenched (denoted by *Q*) and calcined (denoted by *C*) samples of $(La_{0.7}Sr_{0.3})_{0.95}CrO_3$. Quenched samples were heated at 2 °C/min to the indicated temperatures and then quenched in air. Calcined samples were heated at 5 °C/min, held at temperature for 1 h, and subsequently cooled at 5 °C/min to room temperature.

loss whereas subsequent cooling and re-heating of the same sample showed no additional loss in weight. Presumably if CrO_3 volatilization, known to occur above 1000 °C [1], was responsible for the observed weight loss, additional weight loss would have occurred on the second heating. The weight reduction might otherwise be explained by the reintroduction of the $SrCrO_4$ phase into the perovskite structure ($LaCrO_3$) as the temperature increases. XRD of $x = 0.95$ samples indicates a gradual decrease of $SrCrO_4$ with increased temperature (800–1600 °C) as indicated in Fig. 3 and Table I. Chick *et al.* [12] also found that $CaCrO_4$ was reintroduced into the perovskite structure in Ca-doped $LaCrO_3$ with increased firing temperature. Redissolution of $SrCrO_4$ into the perovskite occurs according to the following equation (Kroeger-Vink notation [24]):

$$(1-a)La^{x}_{(0.7/(1-a))}Sr'_{((0.3-a)/(1-a))}Cr^{x}_{(0.7/(1-a))}Cr^{\cdot}{}_{((0.3-a)/(1-a))}O_3 + aSrCrO_4 \longrightarrow La^{x}_{0.7}Sr'_{0.3}Cr^{x}_{0.7}Cr^{\cdot}{}_{0.3}O_3 + a/2O_2 \quad (1)$$

Redissolving Sr into the perovskite requires a reduction of Cr^{6+} to Cr^{3+} and the loss of 1.5 oxygen atoms for every Sr-Cr "molecule" redissolved. For $x = 0.95$ the recorded weight loss from 800 °C to 1200 °C is approximately 0.8 wt %. Semi-quantitative phase analysis of this composition indicates a 4.7 wt % reduction of $SrCrO_4$ over the same temperature range, as indicated in Table I. If we assume that all of this phase has redissolved into the perovskite then this would result in an overall sample weight loss of 0.7 wt % which is almost identical to the decrease in weight observed. Sustained gradual weight loss after the $SrCrO_4$ has melted is presumably due to the continued redissolution of $SrCrO_4$ (now liquid) into the perovskite structure.

XRD was also conducted on powder samples of the LSC-30 $x = 0.95$ that were calcined for one hour and then slow cooled in the furnace. These studies were conducted at 100 °C intervals from 800 °C to 1600 °C to determine if different phase phenomena may be responsible for the unexpectedly high densities achieved during sintering. Fig. 5 compares XRD traces for both calcined and quenched LSC-30 $x = 0.95$ samples between 1000 and 1400 °C. The phases present at each temperature are essentially the same, though the calcined powder indicates larger proportions of unidentified phases at 1200 °C. However, by 1400 °C only trace amounts of Cr_2O_3 are detected in the calcined powder and this cannot account for the high sintered density. As such, it seems most likely that solid state sintering at high temperature (1500–1700 °C) for two hours may be responsible for the high densities achieved.

3.1.3.2. $(La_{0.7}Sr_{0.3})CrO_3$ ($x = 0.99$ and 1.00). Both shrinkage and density measurements indicate that these compositions exhibit very similar sintering characteristics. They produce the highest densities of all the compositions after sintering for 2 h at 1700 °C, and both exhibit two well defined liquid phase sintering events. DTA and TGA analysis of LSC-30 $x = 1.00$, shown in Fig. 6, verifies the first liquid formation at 1256 °C, the melting point of $SrCrO_4$. This data is virtually identical to that obtained for LSC-30 $x = 0.95$, shown in Fig. 4. It indicates gradual oxygen loss from 800 °C to 1500 °C due to a Cr^{6+} to Cr^{3+} reduction as $SrCrO_4$ redissolves into the $LaCrO_3$ perovskite phase, and a small, rapid weight loss resulting from further Cr^{6+} to Cr^{3+} reduction, and oxygen evolution upon incongruent melting of $SrCrO_4$ to liquid and Cr_2O_3. An endotherm associated with the second sintering event occuring in LSC-30 $x = 1.00$ at 1540 °C is not observed in Fig. 6 because it occurs above 1500 °C, the maximum operating temperature of the DSC. One observable difference between

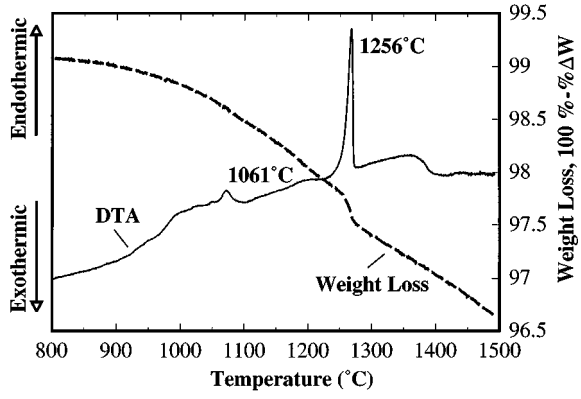

Figure 6 DTA and TGA curves for $La_{0.7}Sr_{0.3}CrO_3$ indicating the melting of $SrCrO_4$ at 1256 °C.

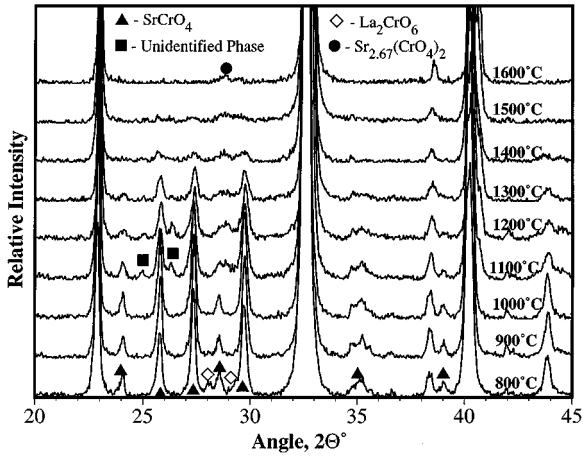

Figure 7 X-ray diffraction patterns of quenched $La_{0.7}Sr_{0.3}CrO_3$ between 22–45° 2Θ indicating non-perovskite phases present from 800–1600 °C.

$x = 0.95$ and 1.00 is the appearance of a small endothermic peak around 1060 °C. This corresponds to a small kink in the shrinkage curve for LSC-30 $x = 1.00$ (Fig. 1), which is a more prominent feature in A-site enriched samples, and may be related to the presence and decomposition of La_2CrO_6. XRD indicates the appearance of La_2CrO_6 between 800 and 1000 °C after which it disappears from X-ray detection as shown in Table I. The relevance of La_2CrO_6 will be addressed in greater detail with reference to the A-site enriched samples in which it is more abundant.

In an attempt to determine phenomena responsible for the second shrinkage event it is necessary to carefully consider phases detected by XRD for these compositions. Fig. 7 shows XRD data for LSC-30 $x = 1.00$ from 800 °C to 1600 °C and between 20–45° 2Θ. Of significant interest is the appearance of trace amounts of another strontium chromate phase, $Sr_{2.67}(CrO_4)_2$ (presumably the formula might also be written as $Sr_4(CrO_4)_3$). This phase has previously been observed by Hartl and Braungart [25] as black hexagonal platelets on strontium oxide growing in the presence of Cr (III) oxide and air at temperatures from 1250–1400 °C. $Sr_{2.67}(CrO_4)_2$ is detected by XRD from 1100–1600 °C for $x = 1.00$ and 1300–1600 °C for $x = 0.99$. The stoichiometric composition $x = 1.00$ contains slightly more of this phase than LSC-30 $x =$

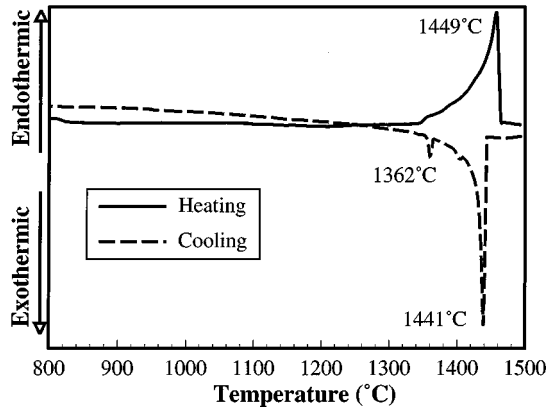

Figure 8 DTA data indicating melting and recrystallization temperatures for in-house produced $Sr_{2.67}(CrO_4)_2$.

0.99. $Sr_{2.67}(CrO_4)_2$ occurs in greater abundance for samples where $x > 1.00$. $Sr_{2.67}(CrO_4)_2$ is not shown in the $SrO\text{-}Cr_2O_3$ phase diagram. The closest related compound on the phase diagram is $Sr_3Cr_2O_8$ [22]. However, XRD data does not exist for $Sr_3Cr_2O_8$, and the closest known compound for which XRD data can be found is $Sr_3Cr_2O_7$. These two discrepancies suggest that there may be some inaccuracies in the published $SrO\text{-}Cr_2O_3$ phase diagram. X-ray phase pure $Sr_{2.67}(CrO_4)_2$ was produced in-house by reacting a stoichiometric powder mixture (ball milled in isopropanol for 24 h) of $SrCO_3$ and Cr_2O_3 at 1350 °C for 1 h in a Pt crucible. DTA analysis of the reacted powder is shown in Fig. 8. It reveals an endotherm around 1449 °C on heating, believed to be the melting of $Sr_{2.67}(CrO_4)_2$, and an exotherm for recrystallization at 1441 °C on cooling. A small exotherm at 1362 °C may be associated with an impurity phase not detected by X-ray.

The XRD trace in Fig. 7 shows the evolution and partial disappearance of the non-perovskite phases in LSC-30 $x = 1.00$. The trace for $x = 0.99$ is similar to this with a slight decrease in the proportion of the $Sr_{2.67}(CrO_4)_2$ phase observed and the presence of trace Cr_2O_3 above 1300 °C. The trace in Fig. 7 indicates the disappearance of La_2CrO_6 by 900 °C, the gradual reduction in the amount of $SrCrO_4$ as it redissolves into the $LaCrO_3$ perovskite with increased temperature, and the evolution of the higher melt temperature $Sr_{2.67}(CrO_4)_2$ phase at 1100 °C, and which is still present in small amounts even at 1600 °C.

No additional phases were detected by XRD to account for liquid melting and densification above 1500 °C. To investigate if the two strontium chromate phases may interact to from a higher melting point phase a 50–50 wt % mixture of $SrCrO_4$ and $Sr_{2.67}(CrO_4)_2$ was analyzed by DTA. Endotherms were observed at 1230 and 1405 °C. Hence it is not possible to explain the high temperature melting by interaction of $Sr_{2.67}(CrO_4)_2$ and $SrCrO_4$. With no evidence of higher melt temperature phases we speculate that the $Sr_{2.67}(CrO_4)_2$ phase is most likely responsible for the second densification event. While this phase may melt from at 1450 °C, XRD indicates only trace amounts are present. Such small amounts of liquid may not be able to dissolve sufficient solid, a requirement during

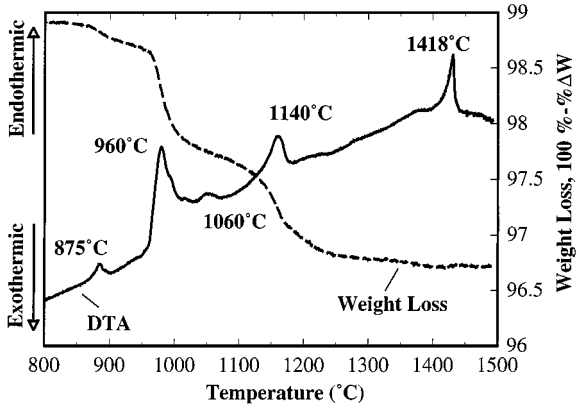

Figure 9 DTA and TGA curves for $(La_{0.7}Sr_{0.3})_{1.05}CrO_3$ indicating major endotherms at 960, 1140 and 1418 °C.

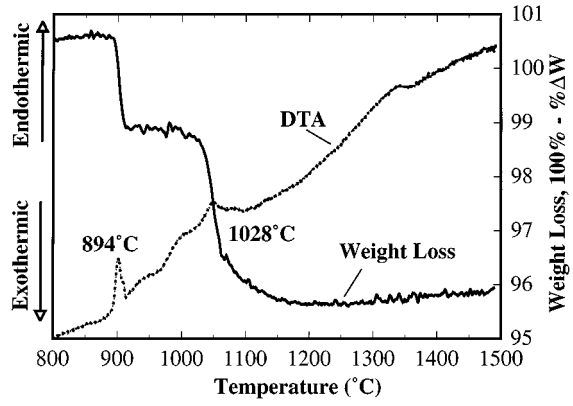

Figure 10 DTA and TGA data for La_2CrO_6 produced by combustion synthesis.

the rapid stages of liquid phase sintering. Increases in temperature may increase the solid solubility in the $Sr_{2.67}(CrO_4)_2$ liquid and also decrease the viscosity of the liquid to the point where rapid densification can take place. Fig. 1 shows the second rapid event occurs at 1540 °C in LSC-30 $x = 1.00$ and 1580 °C in LSC-30 $x = 0.99$. The increase of temperature for $x = 0.99$ may be associated with the fact that this composition contains less $Sr_{2.67}(CrO_4)_2$ liquid and also the presence of trace Cr_2O_3 (an expected second phase in a Cr-rich composition), which may also be dissolved in the liquid, and potentially reduce the amount of additional solid that can be dissolved.

This theory might also be supported by the fact that while shrinkage analysis (Fig. 1) indicates the second shrinkage event occurs at 1540 °C in the LSC-30 $x = 1.00$ sample, sintered density measurements display a sharp increase in density between 1400–1500 °C (Fig. 2). This suggests that the process responsible for densification may be kinetically retarded. On heating at 2 °C per min in the dilatometer there may be insufficient time for the small amount of liquid to wet and dissolve appreciable amounts of solid to facilitate rapid sintering. Longer sintering times may allow dissolution of solid into the $Sr_{2.67}(CrO_4)_2$ phase more readily.

3.1.3.3. $(La_{0.7}Sr_{0.3})_xCrO_3$ ($x = 1.01$, 1.03 and 1.05). Fig. 9 shows thermal data recorded for an LSC-30 $x = 1.05$ composition. Three principal endothermic events are indicated at 960, 1140 and 1418 °C which correspond well with the temperatures at which rapid shrinkage occurs in the A-site enriched samples. Two smaller endotherms are also apparent at 875 and 1060 °C.

All compositions with $x \geq 0.99$ contain La_2CrO_6 between 800–1000 °C (Table I), and observed endotherms around 875 and 1060 °C are believed to be associated with the decomposition of this compound. Berjoan [26] reports that under an oxidizing atmosphere La_2CrO_6 begins to decompose into $LaCrO_3$ and $La_{16}Cr_7O_{44}$ at 950 °C and transforms into them completely by 1050 °C. DTA and TGA of La_2CrO_6, Fig. 10, produced in-house by combustion synthesis, indicate two exothermic events at 894 and 1028 °C and corresponding weight losses at both these temperatures. XRD of La_2CrO_6 heated to 950 and 1100 °C, held for one hour and then quenched in water suggest a different decomposition to that suggested by Berjoan [26]. At 900 °C XRD indicates partial decomposition of La_2CrO_6 to $LaCrO_3$. No $La_{16}Cr_7O_{44}$ was detected, though this may be present in proportions too small to be detected by X-rays. At 1100 °C, the decomposition of the La_2CrO_6 is complete with the formation of $LaCrO_3$ (65 wt %) and La_2O_3 (35 wt %). The weight losses observed at each of these temperatures in Fig. 10 are associated with O_2 loss due to Cr^{6+} to Cr^{3+} reduction as La_2CrO_6 progressively decomposes to $LaCrO_3$.

$$La_2CrO_6 \longrightarrow LaCrO_3 + 1/2La_2O_3 + 3/4O_2 \qquad (2)$$

The decomposition temperatures and weight losses recorded by DTA-TGA for pure La_2CrO_6 (Fig. 10) correspond fairly well with the endotherms and weight losses observed for the LSC-30 $x = 1.05$ sample at 875 and 1060 °C in Fig. 9. Thus it is possible that these thermal events are to some degree associated with La_2CrO_6 decomposition reactions.

In an attempt to explain the endotherm observed around 960 °C, thermal analysis was performed on a mixture of $SrCrO_4$ and La_2CrO_6 since these two compounds co-exist in fairly significant amounts in the A-site enriched LSC-30 compositions from 800–1000 °C. DTA and TGA data for 80 wt % $SrCrO_4$-20 wt % La_2CrO_6 are shown in Fig. 11, and indicates 3 endotherms at 944, 995 and 1230 °C. A significant weight loss is recorded around 950 °C which accurately corresponds to the weight loss observed for the LSC-30 $x = 1.05$ sample in Fig. 9. It is reasonable to conclude that the observed endotherm and associated weight loss at 950 °C in Fig. 9 are the result of interaction between $SrCrO_4$ and La_2CrO_6.

To investigate possible phase interactions between $SrCrO_4$ and La_2CrO_6, X-ray analysis was performed on 80 wt % $SrCrO_4$-20 wt % La_2CrO_6 mixtures heated to 1050 and 1300 °C, held for 1 h and then quenched in water. These results are presented in Table II. The percent by weight of phases listed are essentially the same at both 1050 and 1300 °C indicating that any reactions are completed by 1050 °C. As expected La_2CrO_6 decomposes to $LaCrO_3$. We would also expect to see La_2O_3

TABLE II Phases formed after reacting 80 wt % $SrCrO_4$ + 20 wt % La_2CrO_6 at 1050 and 1300 °C for 1 h

	Actual wt % of all identified phases	Wt % ratio of $SrCrO_4$ to $Sr_{2.67}(CrO_4)_2$
Starting mixture	80 $SrCrO_4$	100 $SrCrO_4$
	20 La_2CrO_6	0 $Sr_{2.67}(CrO_4)_2$
1050 °C, 1 h	23 $SrCrO_4$	42 $SrCrO_4$
	31 $Sr_{2.67}(CrO_4)_2$	58 $Sr_{2.67}(CrO_4)_2$
	46 $LaCrO_3$	
1300 °C, 1 h	25 $SrCrO_4$	41 $SrCrO_4$
	35 $Sr_{2.67}(CrO_4)_2$	59 $Sr_{2.67}(CrO_4)_2$
	40 $LaCrO_3$	

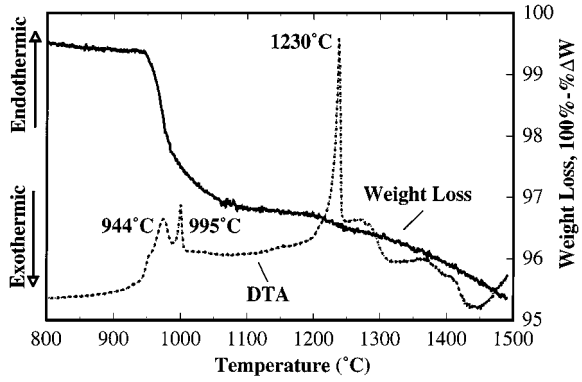

Figure 11 DTA and TGA data for a mixture of 20 wt % $SrCrO_4$ and 80 wt % La_2CrO_6.

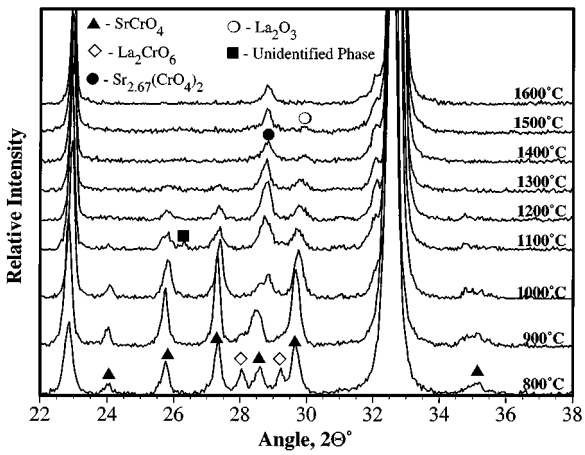

Figure 12 X-ray diffraction patterns of quenched $(La_{0.7}Sr_{0.3})_{1.05}CrO_3$ from 22–38 ° 2Θ indicating non-perovskite phase present between 800–1600 °C.

though this may be present in undetectable amounts, or its formation may have been suppressed by the presence of $SrCrO_4$ in the starting mixture. More interesting is the partial decomposition at 1050 °C of $SrCrO_4$ to $Sr_{2.67}(CrO_4)_2$. This decomposition is also apparent in Fig. 12, showing X-ray data for quenched LSC-30 $x = 1.05$ samples which indicates a significant decrease in the proportion of non-perovskite $SrCrO_4$ between 900–1100 °C. In the same temperature range $Sr_{2.67}(CrO_4)_2$ appears.

The La_2CrO_6-$SrCrO_4$ decomposition reaction presents a plausible explanation for the appearance of $Sr_{2.67}(CrO_4)_2$ in LSC-30 compositions where $x \geq 0.99$. A similar reaction between $CaCrO_4$ and La_2CrO_6 is suggested for Ca-doped $LaCrO_3$. Sakai *et al.* [27] indicate that $CaCrO_4$ and La_2CrO_6 react to form $La_{1-x}Ca_xCrO_3$ and a calcium oxychromate compound of the type $Ca_m(CrO_4)_n$ where $m > n$. Their work implies that the most plausible $Ca_m(CrO_4)_n$ composition would be $Ca_3(CrO_4)_2$ though such a phase was not detected by X-ray at room temperature. Chick *et al.* [12] propose that the melting of a $Ca_m(CrO_4)_n$ type phase, most probably $Ca_3(CrO_4)_2$, was responsible for a second rapid shrinkage event observed around 1200 °C for A-site enriched Ca-doped $LaCrO_3$.

XRD of LSC-30 indicates that all compositions of $x \geq 0.99$ contain La_2CrO_6 around 800–1000 °C, and the presence of this appears to drive decomposition of $SrCrO_4$ to $Sr_{2.67}(CrO_4)_2$. $Sr_{2.67}(CrO_4)_2$ may be a decomposition product because La_2CrO_6 removes chromium from $SrCrO_4$ to form a more thermodynamically stable $LaCrO_3$. Hence $SrCrO_4$ is transformed into the Cr-depleted compound $Sr_{2.67}(CrO_4)_2$. The amount of $Sr_{2.67}(CrO_4)_2$ formed in each composition seems dependent on the initial proportion of La_2CrO_6 at 800 °C. For each composition, $x = 0.95$–1.05, the amount of $SrCrO_4$ at 800 °C is approximately equal (∼10 wt %) whereas the amount of La_2CrO_6 increases with A-site enrichment. Larger amounts of the La_2CrO_6 appear to cause increased $SrCrO_4$ decomposition. Compositions LSC-30 $x = 0.95$ and 0.97, in which no La_2CrO_6 was detected by XRD, do not indicate the presence of $Sr_{2.67}(CrO_4)_2$.

In summary, interactions between La_2CrO_6 and $SrCrO_4$ result in the complete decomposition of La_2CrO_6 predominantly to $LaCrO_3$ and the partial decomposition of $SrCrO_4$ to $Sr_{2.67}(CrO_4)_2$. This decomposition takes place between 900–1100 °C. The weight loss observed at 960 °C in Fig. 9 is most likely associated with this decomposition and results from chromium reduction; La_2CrO_6 to $LaCrO_3$ and $SrCrO_4$ to $Sr_{2.67}(CrO_4)_2$.

While the previously discussed decomposition reactions account for the endotherm and associated weight loss observed for the LSC-30 $x = 1.05$ sample at 960 °C (Fig. 9), no low melting temperature phases were detected by X-ray to explain the rapid shrinkage event occurring at this temperature. However, it is possible that during decomposition some form of particle rearrangement takes place to account for the comparatively small shrinkage observed.

The endotherm and weight loss observed at 1140 °C for LSC-30 $x = 1.05$ coincide with the second rapid shrinkage event for the A-site enriched samples. Although this temperature is 110 °C below the melting temperature of pure $SrCrO_4$ it is plausible to suspect that the shrinkage at 1140 °C is associated with the melting of $SrCrO_4$. Referring back to Fig. 11, DTA-TGA trace of $SrCrO_4$-La_2CrO_6, it is apparent that La_2CrO_6, lowers the melting point of the $SrCrO_4$ by approximately 30 °C. Chick *et al.* [12] observed a similar decrease in melting temperature with the addition of La_2CrO_6 to $CaCrO_4$ in their studies on Ca-doped $LaCrO_3$. They suggested that dissolution of a moderate amount of La oxide into the Ca-Cr oxide should increase the entropy of the liquid, thereby lowering the

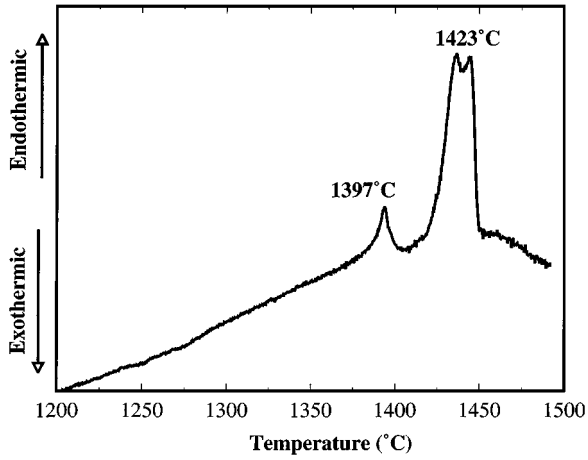

Figure 13 DTA data for a mixture of 70 wt % $Sr_{2.67}(CrO_4)_2$, 15 wt % $SrCrO_4$ and 15 wt % La_2O_3.

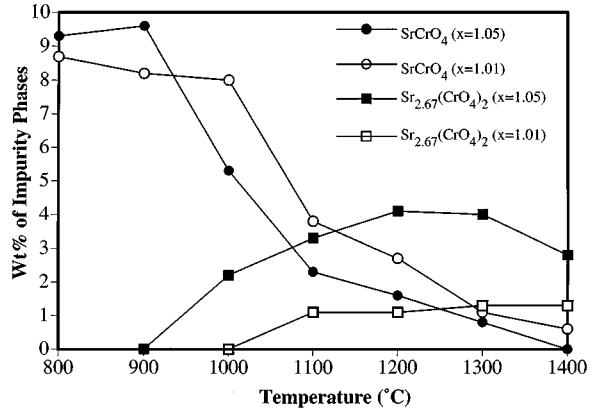

Figure 14 Comparison of the proportions $SrCrO_4$ and $Sr_{2.67}(CrO_4)_2$ in $(La_{0.7}Sr_{0.3})_{1.01}CrO_3$ and $(La_{0.7}Sr_{0.3})_{1.05}CrO_3$ with increasing temperature from 800–1400 °C.

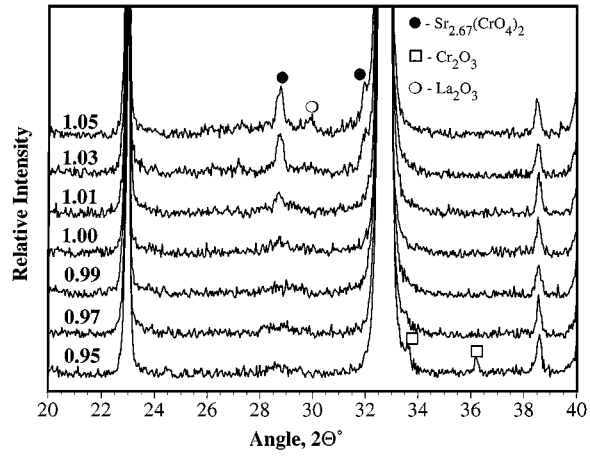

Figure 15 X-ray diffraction patterns of $(La_{0.7}Sr_{0.3})_xCrO_3$ ($0.95 \leq x \leq 1.05$) between 22–40 ° 2Θ indicating non-perovskite phases present after sintering for 2 h at 1600 °C.

melting point. The incorporation of La into the $SrCrO_4$ does not completely explain the 110 °C reduction observed in our studies. However, the additional presence of both $Sr_{2.67}(CrO_4)_2$ and La_2O_3 (Table I) may help to further reduce the melting temperature of $SrCrO_4$. It is also possible that these phases interact to form a peritectic melting point around 1050 °C.

The final shrinkage event observed for A-site enriched samples occurs at ∼1400 °C and is most likely explained by the melting of $Sr_{2.67}(CrO_4)_2$. At this temperature, X-ray data (Table I) indicates the presence of $SrCrO_4$, $Sr_{2.67}(CrO_4)_2$ and La_2O_3. While DTA of in-house produced $Sr_{2.67}(CrO_4)_2$ indicates its melting temperature as ∼1450 °C, the presence of $SrCrO_4$ and La_2O_3 may interact with the $Sr_{2.67}(CrO_4)_2$ to reduce this melting temperature. Fig. 13 shows DTA-TGA data for a mixed sample of 70 wt % $Sr_{2.67}(CrO_4)_2$, 15 wt % $SrCrO_4$ and 15 wt % La_2O_3. This proportion of phases was chosen to reflect the amounts of each phase detected by XRD between 1200–1400 °C. The trace indicates two endotherms at 1396 and 1414 °C which correspond well to the temperature for the third rapid shrinkage event.

Although the shrinkage events for the A-site enriched samples occur at the same temperatures, the two most significant shrinkages vary considerably in magnitude depending on the extent of A-site enrichment. Shrinkage at 1150 °C decreases with A-site enrichment whereas shrinkage at 1400 °C increases with A-site enrichment. The magnitude of the 1150 °C event is possibly related to the amount of $SrCrO_4$ present at the temperature of melting and the 1400 °C event similarly related to the proportion of $Sr_{2.67}(CrO_4)_2$. Fig. 14 compares the proportion of these phases, detected by XRD, in LSC-30 $x = 1.01$ and 1.05 samples. At 1100 °C, $x = 1.01$ contains more $SrCrO_4$ presumably because less La_2CrO_6, present at 800–900 °C, has resulted in reduced $SrCrO_4$ decomposition to $Sr_{2.67}(CrO_4)_2$. Thus $x = 1.01$ has a greater volume of $SrCrO_4$ liquid available for sintering. However, at 1400 °C LSC-30 $x = 1.05$ contains more $Sr_{2.67}(CrO_4)_2$ than $x = 1.01$, due to increased La_2CrO_6 interaction with $SrCrO_4$ at 800–900 °C, which results in larger amounts of $Sr_{2.67}(CrO_4)_2$ as a decomposition product. Hence the $x = 1.05$ composition exhibits enhanced shrinkage at 1400 °C.

XRD data previously presented of quenched samples indicates that non-perovskite phases remain even at 1600 °C. Fig. 15 shows X-ray traces for each composition after sintering at 1600 °C for 2 h. As expected, Cr-enriched samples contain Cr_2O_3 as the second phase which increases with the proportion of excess Cr. For A-site enriched LSC, the predominant second phase is $Sr_{2.67}(CrO_4)_2$, which increases with A-site cation enrichment. For the largest A-site excess investigated, LSC-30 $x = 1.05$, La_2O_3 is also present as a second phase. This would limit the application of this particular composition due to hydration of La_2O_3 and subsequent disintegration of the interconnect.

4. Conclusion

The A-site enriched LSC-30 materials considered in this study exhibit rapid shrinkage around 1050 °C. This is attributed to the melting of $SrCrO_4$ even though the melting point of pure $SrCrO_4$ is 1253 °C. The 100 °C reduction in melting point was believed to be the result of La dissolution into the $SrCrO_4$, and possible interaction with other detected phases, such as $Sr_{2.67}(CrO_4)_2$. Almost identical behavior has

been observed in non-stoichiometric Ca-doped $LaCrO_3$ materials. This study indicates that the melting of $Sr_{2.67}(CrO_4)_2$ around 1400 °C is responsible for the second densification event. This compound is produced by a decomposition reaction between $SrCrO_4$ and La_2CrO_6, and is believed to melt at 1450 °C. Possible interaction with other detected compounds, such as La_2O_3, may cause the observed 50 °C reduction in this melting temperature.

The magnitudes of the two densification events in the A-site enriched LSC-30 compositions from this study were found to be dependent on the degree of A-site enrichment. The magnitude of the first rapid shrinkage around 1150 °C decreases with increased A-site enrichment and can be correlated to a lower proportions of $SrCrO_4$ above 1000 °C in the higher A-site enriched compositions. Higher degrees of A-site enrichment result in larger proportions of La_2CrO_6 between 800–1000 °C and hence more $SrCrO_4$ reacts to produce $Sr_{2.67}(CrO_4)_2$, thus leaving less $SrCrO_4$ for densification at 1150 °C. However, a greater amount of $Sr_{2.67}(CrO_4)_2$ is available for densification when it melts at 1400 °C for the samples with a higher degree of A-site enrichment. Thus the magnitude of the second shrinkage event increases with increased A-site enrichment.

LSC-30 compositions with significant A-site depletion (i.e. LSC-30 $x = 0.95$ and 0.97) exhibit only one shrinkage event at ∼1250 °C which is due to the melting of $SrCrO_4$. This behavior is similar to A-site depleted LCC. However, the marginally depleted and stoichiometric LSC-30 compositions, $x = 0.99$ and 1.00, exhibit a type of intermediate behavior. Both compositions exhibit two rapid densification events. The first occurs at 1250 °C due to $SrCrO_4$ melting, and is similar in magnitude to LSC-30 $x = 0.95$ and 0.97 compositions. The second event occurs at 1540 °C for $x = 1.00$ and 1580 °C for $x = 0.99$. Both compositions contain small amounts of La_2CrO_6 at 800 °C, similar to the A-site enriched compositions investigated. As such, their shrinkage behavior might be expected to resemble that of the A-site enriched samples; i.e. rapid shrinkage around 1150 and 1400 °C. Concerning the first rapid shrinkage, the amount of La_2CrO_6 in samples $x = 0.99$ and 1.00 may be insufficient to reduce the melting temperature of $SrCrO_4$. La_2CrO_6 is also consumed by reaction with $SrCrO_4$ to produce $Sr_{2.67}(CrO_4)_2$ which is detected in both the $x = 0.99$ and 1.00 compositions by X-ray diffraction. If the majority of the La_2CrO_6 is consumed in this reaction, there may be insufficient left to dissolve into the $SrCrO_4$ to reduce its melting temperature. Hence, the first shrinkage event for these compositions occurs at 1250 °C (the melting point of pure $SrCrO_4$). Concerning the higher temperature shrinkage event observed in $x = 0.99$ and 1.00 compositions, XRD indicates that $Sr_{2.67}(CrO_4)_2$ is present in very small proportions in these samples, and this amount is possibly insufficient to cause rapid densification at the temperature of melting ∼1450 °C. Higher temperatures may be required to improve the solid solubility, viscosity and wetting behavior of this liquid to enable liquid phase sintering.

Acknowledgements

The authors appreciate the assistance of David Devir for powder synthesis and Todd Hart for DSC analysis on this project. This work was supported by the Federal Energy Technology Center, Office of Fossil Energy, U.S. Department of Energy Under Contract 22407. Pacific Northwest National Laboratory is operated by Battelle Memorial Institute for the U.S. Department of Energy under Contract No. DE-AC06-76RL0 1830.

References

1. D. B. MEADOWCROFT and J. M. WIMMER, *Amer. Ceram. Soc. Bull.* **58**(6) (1979) 610.
2. A. M. ANTHONY, G. BENEZECH, F. CABANNES, M. FAUCHER, M. FOEX, V. LOC and D. YEROUCHALMI, in Proceedings of the Third International Symposium on High-Temperature Technology (Butter-Worths, London, 1967) p. 215.
3. J. W. HALLORAN and H. U. ANDERSON, *J. Amer. Ceram. Soc.* **57** (1974) 150.
4. L. GROUPP and H. U. ANDERSON, *ibid.* **59**(9–10) (1976) 449.
5. B. K. FLANDERMAYER, J. T. DUSEK, P. E. BLACKBURN, D. W. DEES, C. C. MCPHEETERS and R. B. POEPPEL, in Abstracts of 1986 Fuel Cell Seminar, Tucson, AZ, October 1986 (Courtesy Associates, Washington, DC, 1986) p. 68.
6. L. A. CHICK, J. L. BATES, L. R. PEDERSON and H. E. KISSINGER, in Proceedings of the First International Symposium on Solid Oxide Fuel Cells, edited by S. C. Singhal (The Electrochemical Society, Pennington, NJ, 1989) p. 170.
7. L.-W. TAI and P. A. LESSING, *J. Amer. Ceram. Soc.* **74**(1) (1991) 155.
8. W. SCHAFER and R. SCMIDBERGER, in "High Tech Ceramics," edited by P. Vincenzini (Elsevier Science Publishers B. V., Amsterdam, Netherlands, 1987) p. 1737.
9. P. S. DEVI and M. S. RAO, *Mat. Res. Bull.* **28** (1993) 1075.
10. S. HAYASHI, K. FUKAYA and H. SAITO, *J. Mater. Sci. Letts.* **7** (1988) 457.
11. M. R. MORELLI, "Liquid Phase Sintering of Perovskite," D. Phil. Thesis, University of Oxford, U.K., 1995.
12. L. A. CHICK, J. LIU, J. W. STEVENSON, T. R. ARMSTRONG, D. E. MCCREADY, G. D. MAUPIN, G. W. COFFEY and C. A. COYLE, *J. Amer. Ceram. Soc.* **80**(8) (1997) 2109.
13. T. R. ARMSTRONG, J. W. STEVENSON, L. R. PEDERSON and P. E. RANEY, *J. Electrochem. Soc.* **143**(9) (1996) 2919.
14. L. A. CHICK and J. L. BATES, in Proceedings of the Fourth Annual Fuel Cells Contractors Review Meeting, Morgantown, WV, July 14–15, 1992, DOE/METC-92/6127, edited by W. J. Huber (U.S. Department of Energy, Morgantown, WV, 1992) p. 114.
15. D. B. MEADOWCROFT, *Brit. J. Appl. Phys. Ser. 2* **2** (1969) 1225.
16. M. MORI, T. YAMAMOTO, H. ITOH and T. ABE, in Proceedings of the Fourth International Symposium on Solid Oxide Fuel Cells, edited by M. Dokiya, O. Yamamoto, H. Tagawa and S. C. Singhal (The Electrochemical Society, Pennington, NJ, 1995) p. 905.
17. N. M. SAMMES, R. RATNARAJ and M. G. FEE, *J. Mater. Sci.* **29** (1994) 4319.
18. L. A. CHICK, J. L. BATES and G. D. MAUPIN, in Proceedings Second International Symposium on Solid Oxide Fuel Cells, Athens, Greece, July 2–5, 1991, edited by F. Grosz, P. Zegers, S. C. Singhal and O. Yamamoto (Commission of the European Communities, Luxembourg, 1991) p. 629.
19. L. A. CHICK, L. R. PEDERSON, G. D. MAUPIN, J. L. BATES, L. E. THOMAS and G. J. EXARHOS, *Mater. Lett.* **10**(1, 2) (1990) 6.
20. C. N. REILLEY and R. W. SCHMID, *Anal. Chem.* **30** (1957) 947.

21. R. M. GERMAN, S. FAROOQ and C. M. KIPPHUT, *Mat. Sci. and Eng. A* **105/106** (1988) 215.
22. T. NEGAS and R. S. ROTH, *J. Res. Nat. Bur. Stand., Sect. A* **73**(4) (1969) 431.
23. J. D. CARTER, M. M. NASRALLAH and H. U. ANDERSON, *J. Mater. Sci.* **31** (1996) 157.
24. F. A. KROEGER, "The Chemistry of Imperfect Crystals" (North-Holland, Amsterdam, 1964).
25. K. HARTL and R. BRAUNGART, *Z. Naturforsch* **33b** (1978) 952.
26. R. BERJOAN, *Rev. Int. Hautes Temp. Refract.* **13** (1976) 119.
27. N. SAKAI, T. KAWADA, H. YOKOKAWA, M. DOKIYA and I. KOJIMA, *J. Amer. Ceram. Soc.* **76**(3) (1993) 609.

Received 27 January
and accepted 23 June 1999